Preparation and Study of Decavanadate-Pillared Hydrotalcite-like Anionic Clays Containing Cobalt and Chromium

M. del Arco,[†] M. V. G. Galiano,[†] V. Rives,*[,†] R. Trujillano,[†] and P. Malet[‡]

Departamento de Química Inorgánica, Facultad de Farmacia, Universidad de Salamanca, Salamanca, Spain, and Departamento de Química Inorgánica, Facultad de Química, Instituto de Ciencia de Materiales, Centro Mixto CSIC, Universidad de Sevilla, Sevilla, Spain

Received February 9, 1996[⊗]

Hydrotalcite-like compounds containing Co(II) and Cr(III) in the brucite-like layers have been prepared. The interlayer anion was carbonate or decavanadate. The chemical formulas of the samples are $[Co_{0.65}Cr_{0.35}(OH)_2](CO_3)_{0.175}\cdot 1.22H_2O$ (sample CoCrC) and $[Co_{0.61}Cr_{0.39}(OH)_2](V_{10}O_{28})_{0.065}\cdot 1.35H_2O$ (sample CoCrV). The compounds have been characterized by X-ray diffraction, XAS, vis-UV, FT-IR, and Raman spectroscopies, while the surface textures were assessed by nitrogen adsorption. Reducibility has been studied by temperature-programmed reduction. A similar characterization study has been carried out on samples obtained after calcination of the parent samples in air at increasing temperatures. Results indicate an ordered structure, with Co(II) and Cr(III) ions in octahedral holes of the brucite-like layers and, in CoCrV, decavanadate species with its main C_2 axis parallel to the layers. Thermal decomposition at increasing temperatures takes place, for CoCrC, through intermediate formation of Cr(VI) species, which are again reduced to Cr(III) at higher temperatures; simultaneously, Co(II) is oxidized to Co(III) (even at 673 K), thus leading to formation of $Co^{II}Co^{III}Cr^{III}O_4$. However, decomposition of CoCrV takes place through partial depolymerization of decavanadate species and formation of $Co^{II}Cr_2O_4$ and $Co^{II}{}_2V_2O_7$, without intermediate formation of Cr(VI) species.

Introduction

Layered double hydroxides (LDH) are materials with an increasing interest because of the large number of fields where they find applications, such as pharmaceuticals, adsorbents, etc., as well as the use of their decomposition products as catalysts and catalyst supports, mainly in hydrogenation, aldol condensation, re-forming, and also selective oxidation.[1] Probably, the unique advantage of hydrotalcites occurs because the different cations are well apart from each other, thus allowing formation of well-dispersed mixed oxides upon decomposition.

Although they are commonly known as "hydrotalcite-like" compounds, they should be more properly named "anionic clays", as hydroxyl is not (most usually) the only anion existing in the structure. Their formula can be written as $[M_{1-x}M'_x(OH)_2]^{x+}(X^{m-})_{x/m}\cdot nH_2O$, where M = divalent cation, M′ = trivalent cation, X = anion, usually Cl^-, OH^-, CO_3^{2-}, and carboxylate, etc. The name comes from the mineral hydrotalcite, $Mg_6Al_2(OH)_{16}(CO_3)\cdot 4H_2O$, or $[Mg_{0.75}Al_{0.25}(OH)_2](CO_3)_{0.125}\cdot 0.5H_2O$, according to the formulation method above given. Their structure consists of brucite-like layers positively charged after partial M(II)/M′(III) substitution, the excess in positive charge being balanced by interlayer anions; water molecules also are located in the interlayers. One of the most useful properties of hydrotalcites is the easy exchange of the interlayer anions, leading to a large number of different compounds. Exchange of carbonate, chloride, nitrate, etc., with polyoxometallates may lead to formation of pillared materials.

One of the methods reported in the literature for exchanging the interlayer anion is based on the ability of LDH to recover their layered structure after a mild calcination (*ca*. 700 K, depending on the nature of the ions in the layers) when immersed in aqueous solutions containing the entering anion.[2] Bish[3] has described another method consisting of reaction of the LDH with dilute HCl; this reaction gives rise to decomposition of carbonate (because of the lower pH) and introduction of chloride in the interlayers; chloride is more easily exchanged than carbonate, and then a further exchange may lead to the desired compound. This reaction can be summarized as follows:

$$[LDH]CO_3 + 2HCl \rightarrow [LDH]Cl_2 + CO_2 + H_2O$$

This method has been successfully used by Kwon *et al*.[4] and Woltermann[5] to introduce decavanadate, $V_{10}O_{28}^{6-}$, in hydrotalcites containing Zn−Al, Zn−Cr, or Ni−Al in the brucite-like layers. Drezdzon[6] has reported that the procedure is even easier if the interlayer is previously expanded by introduction of organic molecules such as terephtalate. Ulibarri *et al*.[7] have recently reported a comparative study on the use of different methods to intercalate decavanadate into hydrotalcite (*i.e*., direct exchange, intermediate use of terphtalate, and reconstruction from the product calcined at 823 K).

Preparation of mixed oxides containing two or three different cations is a very interesting field, as these sorts of materials find application in reactions involving catalytic partial and selective oxidation processes. The use of hydrotalcites seems rather interesting in this field, because, with use of different atomic ratios, the chemical composition of the layers can be changed; moreover, the introduction of interlayer polyoxometallates is then a method for introducing a third cation in the mixed oxide obtained after calcination of the resulting exchanged hydrotalcite.

* Author to whom correspondence should be addressed.
† Universidad de Salamanca.
‡ Universidad de Sevilla.
⊗ Abstract published in *Advance ACS Abstracts,* September 15, 1996.

(1) Cavani, F.; Trifiro, F.; Vaccari, A. *Catal. Today* **1991**, *11*, 1.
(2) Reichle, W. T. *Solid State Ionics* **1986**, *22*, 135.
(3) Bish, D. L. *Bull. Mineral.* **1980**, *52*, 1036.
(4) Kwon, T.; Tsigdinos, A.; Pinnavaia, T. J. *J. Am. Chem. Soc*. **1988**, *110*, 3653.
(5) Woltermann, G. M. U. S. Patent 4, 454, 244, 1988.
(6) Drezdzon, M. A. *Inorg. Chem*. **1988**, *27*, 4628.
(7) Ulibarri, M. A.; Labajos, F. M.; Rives, V.; Trujillano, R.; Kagunya,W.; Jones, W. *Inorg. Chem.* **1994**, *33*, 2592.

S0020-1669(96)00155-3 CCC: $12.00

In the present work we report on the preparation of a material possessing the hydrotalcite-like structure containing cobalt and chromium in the layers and carbonate in the interlayers. From this, another layered material has been prepared by exchange of the interlayer carbonate with decavanadate, using the intermediate reaction with HCl. Finally, the thermal decomposition of both solids to mixed oxides has been monitored.

Experimental Section

Samples Preparation. The layered materials have been prepared following the method described in the literature.[2] All reagents were from Fluka, p.a. (Germany). An aqueous solution containing 30 g of $Co(NO_3)_2 \cdot 6H_2O$ (*ca*. 0.1 mol) and 21 g of $Cr(NO_3)_3 \cdot 9H_2O$ (*ca*. 0.05 mol) in 300 mL of distilled water was slowly added at room temperature to another solution containing 12 g of NaOH (*ca*. 0.3 mol) and 5.5 g of Na_2CO_3 (*ca*. 0.05 mol) in 500 mL of distilled water, while this was being vigorously magnetically stirred. Once the addition was completed, the purple suspension was stirred for 24 h at room temperature. The precipitate was separated by centrifugation and washed with distilled water until the washings were free of nitrate.[8] A portion of the suspension was filtered and dried at room temperature, leading to a sample named hereafter CoCrC. A portion of 100 mL of the suspension (containing *ca*. 4 g of solid) was adjusted to pH 4.5 with 0.5 M HCl. An aqueous solution was prepared by dissolving 4 g of $NaVO_3$ in 100 mL of water, and it was also adjusted to pH 4.5 using 0.5 M HCl. The suspension of the hydrotalcite was introduced in a Dosimat 725 coupled to a pH-meter Model 691, and the vanadate solution was slowly added (*ca*. 30 drops/min), the pH being automatically maintained at a value of 4.5. Once the addition had been completed, the system was stirred at room temperature for 48 h, the pH being automatically maintained at 4.5 during all of the procedure. The solid thus obtained was centrifuged and washed until no free (unexchanged) vanadate remained, thus leading to a sample named CoCrV.

Both layered precursors, CoCrC and CoCrV, were heated in air for 2 h at increasing temperatures, leading to samples named CoCoC-*T* and CoCrV-*T*, respectively, where T stands for the calcination temperature in kelvin.

Techniques. Chemical analysis for Co, Cr, and V were carried out by atomic absorption in a Mark-II ELL-240 instrument. Analysis for C was performed in a Perkin-Elmer 2400 CHN apparatus.

X-ray diffraction (XRD) patterns were recorded on a Siemens D-500 diffractometer with a graphite-filtered Cu Kα1 radiation (1.5405 Å) and interfaced to a DACO-MP data acquisition microprocessor provided with Diffract/AT software.

Differential thermal analysis (DTA) and thermogravimetric analysis (TGA) of the samples were carried out in Perkin-Elmer DTA 1700 and TGS-2 apparatuses, respectively, coupled to a Perkin-Elmer 3600 data station, at a heating rate of 10 K/min.

The visible−ultraviolet spectra of the samples were recorded following the diffuse reflectance technique (vis−UV/DR) in a Shimadzu UV-240 spectrophotometer, using 5 nm slits and MgO as a reference.

Specific surface areas were measured following the single-point method in a Micromeritics Flowsorb II-2300 apparatus by nitrogen adsorption after degassing the samples *in situ* at 400 K for 2 h. Full nitrogen-adsorption isotherms were recorded in a Pyrex high-vacuum instrument, equipped with a rotary pump, silicon oil diffusion pump, and McLeod gauge for absolute pressure measurement; changes in pressure during adsorption were monitored with an MKS pressure transducer; the samples were outgassed *in situ* at 400 K for 2 h before the isotherm was recorded.

The Fourier-transform infrared spectra (FT-IR) of the samples were recorded in a Perkin-Elmer FT-IR 1730 apparatus, with a nominal resolution of 2 cm^{-1} and averaging 100 scans; the sample was pressed in KBr pellets.

Temperature-programmed reduction (TPR) analysis was carried out in a Micromeritics TPR/TPD 2900 instrument, at a heating rate of 10 K/min, and using *ca*. 15 mg of sample and a H_2/Ar (5% vol) mixture (from Sociedad Española del Oxígeno, Spain) as reducing agent (60 mL/min); experimental conditions for TPR runs were chosen according to data reported elsewhere[9] in order to reach good resolution of the component peaks.

Table 1. Results of Chemical Analysis (Metals) for Samples CoCrC and CoCrV

sample	Co[a]	Cr[a]	V[a]	C[a]	Co/Cr[b]	S_{BET}[c]
CoCrC	29.5	14.0		1.73	1.86	86
CoCrV	18.3	10.4	18.7	0.02	1.60	94

[a] Weight percent. [b] Atomic ratio. [c] Unit: $m^2\ g^{-1}$.

The laser-Raman spectra were recorded in a FT-Raman 910 instrument from Nicolet, using a Nd laser (9394 cm^{-1}) and a Ge detector.

X-ray absorption spectra (XAS) at the V K (5464 eV), Cr K (5989 eV), and Co K (7710 eV) edges were collected at 77 K on station 8.1 at Daresbury Synchrotron Radiation Source (Daresbury, U.K.) with an electron ring running at 2 GeV and 150−210 mA. Monochromatization was obtained with a double silicon crystal monochromator working at the (111) reflection, which was detuned 20% to minimize higher harmonics. The measurements were carried out in transmission mode using optimized ion chambers as detectors. The samples were ground and homogenized, diluted with boron nitride when neccessary, and pressed into self-supporting wafers with a total absorbance 2.5 above the recorded edge and edge jumps between 0.4 and 1.0. At least three scans were recorded and averaged in order to obtain the experimental spectra. The EXAFS function ($\chi(k)$) was obtained from the experimental X-ray absortion spectrum by conventional procedures.[10] EXAFS data analysis and handling were performed using the program package NEWEXAFS. Theoretical backscatterering amplitude and phase functions for absorber−backscatterer pairs were calculated by using the program FEFF.[11] *n*-Hexylammonium vanadate used as a reference material in XAS experiments was provided by Román *et al*.[12]

Results and Discussion

Cobalt−Chromium Hydrotalcites. (a) Chemical Analysis. Results for chemical analysis are given in Table 1, where the atomic ratios for the cations in the layers are also given. These are 1.86 and 1.60, respectively, for samples CoCrC and CoCrV, both values being within the usual range reported in the literature for different hydrotalcites.[1] The slight decrease for sample CoCrV should be ascribed to an easier, more selective dissolution of Cr(III) during treatments leading to sample CoCrV.

FT-IR studies (see below) show that carbonate is the only interlayer anion in sample CoCrC, the presence of bicarbonate being excluded because IR bands that could be ascribed to such an anion are absent. On the other hand, FT-IR shows the absence of carbonate in sample CoCrV where only traces of C are detected by elemental chemical analysis, thus indicating that the exchange of CO_3^{2-} by vanadate species has been effective.

With regard to the interlayer anion in sample CoCrV, we assume a general formula $V_\alpha O_\beta^{\gamma-}$ and that all vanadium is present as a single species in the interlayer, balancing the positive charge of the layers. The α/γ ratio can be obtained from the Cr and V contents (Table 1), and the formula of the polyvanadate species can be written as $[V_{10}O_{27.5}]^{5.4-}$, very close to the expected $[V_{10}O_{28}]^{6-}$ that is the stable species at pH = 4.5.[13]

From these data the formulas of these precursors can be written as follows: $[Co_{0.65}Cr_{0.35}(OH)_2](CO_3)_{0.175} \cdot 1.22H_2O$ and

(8) Burriel, F.; Lucena, F.; Arribas, S.; Hernández, J. *Química Analítica Cuantitativa*, 13th ed.; Paraninfo: Madrid, 1989.

(9) Malet, P.; Caballero, A. *J. Chem. Soc., Faraday Trans. 1* **1988**, *84*, 2369.

(10) Sayers, D. E.; Bunker, B. A. in *X-Ray Absorption: Principles, Applications and Techniques of EXAFS, SEXAFS and XANES;* Koningsberger, D. C., Prins, R., Eds.; Wiley: New York, 1988.

(11) Mustre de León, J.; Rehr, J. J.; Zabinsky, S. I.; Albers, R. C. *Phys. Rev. B* **1991**, *44*, 4146.

(12) Román, P.; Aranzabe, A.; Luque, A.; Gutiérrez Zorrilla, J. M. *Mater. Res. Bull*. **1991**, *26*, 731.

(13) Clark, R. J. H. In *Comprehensive Inorganic Chemistry*; Bailar, J. C., Jr., Emeleus, H. J., Nyholm, R., Trotman-Dickenson, A. F., Eds.: Pergamon Press: Oxford, U.K., 1973.

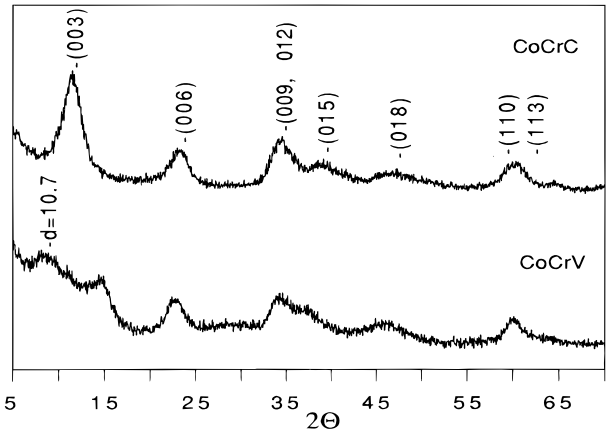

Figure 1. X-ray diffraction patterns of CoCrC and CoCrV hydrotalcites.

$[Co_{0.61}Cr_{0.39}(OH)_2](V_{10}O_{28})_{0.065}\cdot 1.35H_2O$, assuming that the only trivalent cation in the layers is Cr(III) and calculating the water content from TGA (see below).

(b) Structure of Cobalt−Chromium Hydrotalcites. The X-ray diffraction diagrams of samples CoCrC and CoCrV are included in Figure 1. Peaks for sample CoCrC are sharp and intense, although the overall crystallinity is lower than that previously found for Mg, Al hydrotalcites.[14] It should be noted that only peaks due to diffraction by the layered material are recorded, peaks originating from crystalline oxides, hydroxides, carbonates, or bicarbonates of the component cations being absolutely absent; these compounds are usually formed during preparations similar to that used here if too large M(II)/M(III) ratios or prolonged hydrothermal treatment (usually carried out to improve the crystallinity) are used.[14] The spacing measured for planes (003), corresponding to one-third of dimension *c*, is 7.65 Å, within the range reported for different hydrotalcites containing Cr(III) and Zn(II), Cu(II) or Ni(II), and F^-, Cl^-, NO_3^- or CO_3^{2-} in the interlayer.[1,15] On the other hand, parameter *a* is 3.058 Å and is calculated from the position of the XRD peak due to planes (110). This parameter depends only on the nature of the cations existing in the layers, and the value is within the range usually reported for materials with the hydrotalcite structure.[1,15−17]

The diagram for sample CoCrV shows two reflections corresponding to diffraction by planes (006) and (009) at 5.87 and 3.90 Å, respectively, although shifted toward lower diffraction angles than in the case of sample CoCrC. The broad peak at 10.7 Å does not match with the position expected for planes (003) if the peaks at 5.87 and 3.90 Å are ascribed to planes (006) and (009), respectively. Pinnavaia *et al.*[18] have reported a broad peak at 10.2−10.9 Å upon intercalation of $[\alpha\text{-}SiW_{11}O_{39}]^{8-}$ into zinc and aluminum hydrotalcites, and this peak has been ascribed to Zn^{2+} and Al^{3+} salts of the polyoxometallate; Clearfield *et al.*[19] have also reported a broad peak at 11−13 Å for compounds similar to those studied here, and they have ascribed it to a new compound formed as a result of the reaction between the basic hydrotalcite and the acidic polyoxometallate. Ulibarri *et al.*[7] have recorded a peak at 10.4 Å in the XRD diagrams of decavanadate-containing Mg, Al hydrotalcites prepared following different methods, and, in agreement with these authors, it has been ascribed to the presence of a biphasic material that hinders the peak due to diffraction by planes (003). So, the expected position for the peak due to diffraction by planes (003) can be calculated from the positions of the sharper peaks due to the (006) and (009) planes by using the following equation:

$$d_{(003)} = (1/2)[2d_{(006)} + 3d_{(009)}]$$

thus yielding a value of 11.72 Å, *i.e.*, it is probably hidden by the broad peak at 10.7 Å. The value calculated for parameter *c* ($3d_{003} = 35.26$ Å) is in agreement with the value reported by several authors[7,20,21] for decavanadate-containing hydrotalcites. Finally, parameter *a* is 3.08 Å, coincident within experimental error with the value of sample CoCrC.

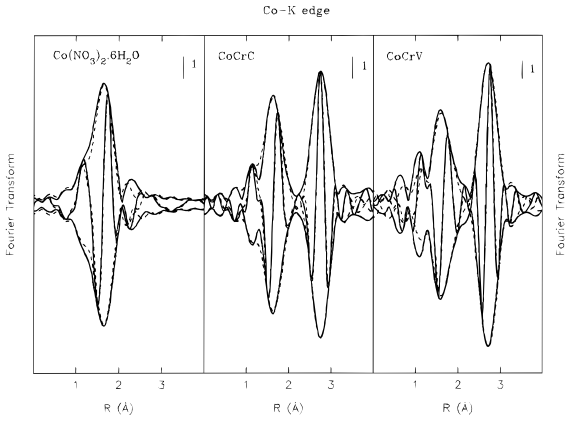

Figure 2. Co K edge EXAFS: Modulus and imaginary part of the k^3-weighted Fourier transform for CoCrC and CoCrV hydrotalcites and for crystalline $Co(NO_3)_2\cdot 6H_2O$. Solid lines: unfiltered experimental data. Dashed lines: best-fit functions. $\Delta k = 3-12$ Å^{-1} in all of the Fourier transforms.

Although both diagrams in Figure 1 show a broad reflection close to $2\theta = 35°$, this cannot be due to the presence of carbonate-containing LDH in sample CoCrV, as the C content in this sample is only 0.02% and, in addition, the more intense peak due to planes (006) is not recorded for sample CoCrV in the position expected for CoCrC.

The pronounced asymmetry of the diffraction peaks due to the (015) and (018) planes has already been reported for samples similar to those prepared in this work[22] and has been ascribed to a partial disordered structure, coexisting with well-ordered stacks of layers.

The local order around the Co and Cr cations in samples CoCrC and CoCrV has been studied by X-ray absorption spectroscopy (XAS) in order to ascertain whether all the cations are located within the layers (the broadening observed in XRD lines thus being produced by the presence of small crystals) or whether amorphous phases are present in addition to the hydrotalcite material. For both samples, the Fourier transform (FT) of the EXAFS oscillations at the Co K edge, Figure 2, has two well-resolved peaks at *ca.* 1.6 and 2.8 Å (phase shift uncorrected). The first peak also appears in the FT of bulk $Co(NO_3)_2\cdot 6H_2O$ and should be ascribed to oxygen neighbors in the first coordination shell of Co. The second maximum appears only for the hydrotalcites, and, in agrement with the structure of the layer (see Chart 1), its main contribution should

(14) Del Arco, M.; Rives, V.; Trujillano, R. *Stud. Surf. Sci. Catal*. **1993**, *87*, 507.
(15) de Roy, A.; Forano, C.; El Malki, K.; Besse, J. P. In *Expanded Clays and Others Microporous Solids*; Occelli, M. L., Robson, H. R., Eds.; Van Nostrand Reinhold: New York, 1992.
(16) Ulibarri, M. A.; Fernández, J. M.; Labajos, F. M.; Rives, V. *Chem. Mater*. **1991**, *3*, 626.
(17) Uzonova, E.; Klissurski, D.; Mitov, I.; Stefanov, P. *Chem. Mater*. **1993**, *5*, 576.
(18) Narita, E.; Kaviratna, P.; Pinnavaia, T. J. *Chem Lett*. **1991**, 805.
(19) Wang, J.; Tiam, Y.; Wang, R. C.; Clearfield, A. *Chem. Mater*. **1992**, *4*, 1276.
(20) Kooli, F.; Rives, V.; Ulibarri, M. A. *Inorg. Chem*. **1995**, *34*, 5114.
(21) Kooli, F.; Rives, V.; Ulibarri, M. A. *Inorg. Chem*. **1995**, *34*, 5122.
(22) Hernández, J. M.; Ulibarri, M. A.; Cornejo, J.; Peña, M. J.; Serna, C. J. *Thermochim. Acta* **1985**, *94*, 257.

Chart 1. Idealized Structure of a Brucite-like Layer Showing Coordination Shells around a Given Cation (Solid Circle): (1) First Coordination Shell of Oxide Anions; (2) Second Coordination Shell of Cations; (3) Third Coordination Shell of Anions

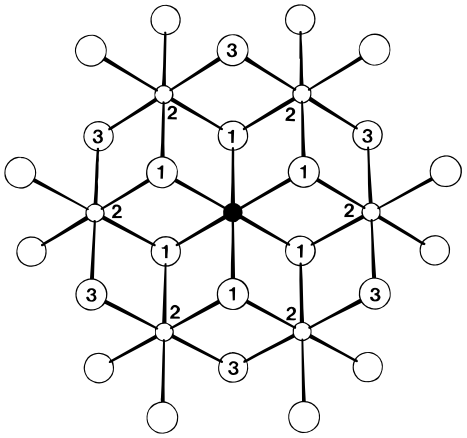

be due to metallic cations forming a second coordination shell at distance *a*. EXAFS spectra were analyzed by best-fit procedures. Fit parameters obtained for $Co(NO_3)_2 \cdot 6H_2O$ (6.0 oxygen atoms at 2.07 Å) are in excellent agreement with crystallographic data for this material (6 oxygen neighbors at 2.066 Å[23]), showing the suitability of theoretical references employed in the analysis.

EXAFS data at the Cr K edge (not shown) are similar to those obtained at the Co K edge, the FT also showing two resolved peaks for CoCrC. EXAFS oscillations at the V K edge for sample CoCrV are only 520 eV lower in energy than the Cr K edge, contaminated Cr K EXAFS oscillations being useless for a proper analysis. However, the XANES region of the Cr K XAS, also sensitive to the local environment of the absorbing atom, is almost identical for CoCrC and CoCrV, thus indicating that the structure around Cr^{3+} cations is the same for both samples. The Cr K EXAFS of an aqueous solution of $Cr(NO_3)_3 \cdot 9H_2O$ was recorded and analyzed to test the suitability of the analysis procedure. Best-fit parameters for the spectrum of this solution (6.1 oxygen neighbors at 1.96 Å) are also in good agreement with the known coordination of Cr^{3+} cations in aqueous solution (6.0 oxygen at 2.0 Å[24]).

In agreement with the coordination expected if all of the metallic cations were within the layers of a hydrotalcite structure (see Chart 1), an excellent fit of the first two maxima appearing in the FT is obtained either at the Co K edge (see Figure 2) or Cr K edge by considering three coordination shells for which fit parameters are collected in Table 2. The first shell of both cations is fitted by 6 ± 0.1 oxygen atoms, indicating that they are located in octahedral sites in an oxygen framework, while the second shell has a main contribution of 6 ± 0.1 metallic atoms at 3.09 ± 0.01 Å. The fit is improved by introducing a weaker contribution of a third shell formed by *ca*. 6 oxygen neighbors at 3.68 Å.

It should be noted here that it is not possible to determine the relative number of Co and Cr cations in the second shell, due to the similar atomic numbers of both elements. Thus, by considering either Co and/or Cr neighbors, we obtained fits with the same quality, changes in the fit parameters being within experimental error.

It is also worth noting that the shortest Co−O bond distance for the CoCrC sample (2.08 Å) is significantly longer than the shortest Cr−O bond distance (1.98 Å), the difference between both M−O distances ($\Delta R = 0.10$ Å) being close to the difference between ionic radii for both cations [$r(Co^{2+}) - r(Cr^{3+}) = 0.12$ Å].[25] This result indicates the existence of distortions in the hydrotalcite layer due to the different cationic radii. EXAFS spectroscopy is sensitive to such distortions, which are not detected by XRD or other experimental techniques.

Table 2. CoCrC and CoCrV Hydrotalcites: Structural Parameters from EXAFS[a]

bond	N	$\Delta\sigma^2 \times 10^3$	R (Å)	$\Delta E°$ (eV)
		CoCrC		
Co−O	6.0	6.9	2.08	3.3
Co−M	6.0	7.2	3.10	2.5
Co−O	5.9	8.5	3.68	3.3
Cr−O	6.0	3.2	1.98	6.8
Cr−M	6.0	6.9	3.09	11.0
Cr−O	7.8	2.2	3.83	10.6
		CoCrV		
Co−O	6.0	5.4	2.08	6.5
Co−M	5.9	4.6	3.08	7.6
Co−O	5.9	8.8	3.68	3.5

[a] Estimated error for coordination numbers (N) and bond lengths (R) are ±10% and ±0.02 Å, respectively. Unfiltered experimental data were fitted (fit range 3−12 $Å^{-1}$ at the Co K edge and 3.4−11.9 $Å^{-1}$ at the Cr K edge).

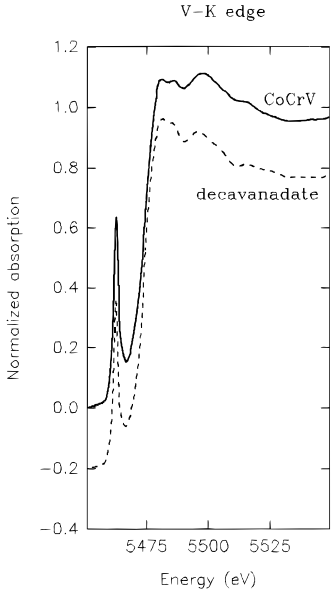

Figure 3. V K edge XANES for hydrotalcite CoCrV and crystalline *n*-hexylammonium decavanadate.

The structure of vanadate ions in the interlayer is also clarified by XAS. Figure 3 shows the XANES at the V K edge for the CoCrV sample compared with that recorded for a crystalline decavanadate [$(n\text{-}C_6H_{13}NH_3)_6(V_{10}O_{28}) \cdot 2H_2O$]. Features such as preedge peak intensity and position, main edge position, and postedge structure are almost identical in both spectra, indicating that vanadium in CoCrV is as V^{5+} forming decavanadate clusters.

(c) Oxidation State of Cobalt. Co(II) is stable in acidic solutions, as the standard electrode potential of the pair $Co_{aq}^{3+}/Co_{aq}^{2+}$ is 1.808 V at pH = 0.[25] However, this value sharply decreases as the pH is increased, reaching a value of 0.17 V at pH = 14. So, an oxidation (partial, at least) oxidation of Co(II) to Co(III) during the precipitation process cannot be

(23) Prelesnik, P. V.; Gabela, F.; Ribar, B.; Kristanovic, I. *Cryst. Struct. Commun.* **1973**, *2*, 581.
(24) Magini, M. *X-Ray Difraction of Ions in Aqueous Solutions*; CRC Press: Boca Raton, FL, 1988.
(25) Huheey, J. E.; Keiter, E. A.; Keiter, R. L. *Inorganic Chemistry, Principles of Stucture and Reactivity*, 4th ed., Harper Collins: New York, 1993.

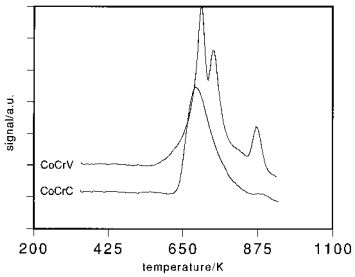

Figure 4. Temperature-programmed reduction curves for hydrotalcites CoCrC and CoCrV.

discarded beforehand. We report here on some studies in order to assess the oxidation state of Co in the samples prepared here.

The position of the main edge in the XAS spectrum is sensitive to the oxidation state of the absorbing atom, being shifted to higher energies when its positive charge increases. The position of the first inflection point at the Co K edge (7718.7 ± 0.1 eV) does not change in a significant way when going from $Co(NO_3)_2 \cdot 6H_2O$ to CoCr hydrotalcites, thus showing that most cobalt is as divalent cations in these samples.

The oxidation state of cobalt has been also ascertained by temperature-programmed reduction (TPR). The reduction profile for sample CoCrC, Figure 4, shows a single, broad reduction step centered at *ca.* 673 K; under the experimental conditions used, Co(II) should be reduced to Co(0), while Cr(III) is not reduced.[26] The recorded hydrogen consumption (5200 μmol H_2/g solid) fits within 4% the amount of cobalt in the sample (5010 μg of atoms/g of solid), thus accounting for the reaction

$$Co^{2+} + H_2 \rightarrow Co + 2H^+$$

We should conclude that no significant oxidation of Co(II) has taken place during synthesis of the hydrotalcite.

With regards to sample CoCrV, the TPR profile shows a reduction peak split in two maxima at 693 and 737 K and an additional peak at 879 K. We have previously reported[26] that V(V) species of interlayer decavanadate is reduced to V(III) under these conditions. Hydrogen consumption was 6940 μmol of H_2/g of solid, a value that fits, within 3%, that required to reduce Co (3110 μg of atoms/g of solid) and V (3660 μg of atoms/g of solid), and so we conclude that no cobalt has been oxidized to Co(III) during preparation of sample CoCrV. The split maximum (the position of which is very close to that of the single peak recorded for sample CoCrC) corresponds to reduction of Co(II) to Co(0), while the weak peak at 879 K is due to V(V) → V(III) reduction. Splitting of the reduction peak due to cobalt is caused by the different nature of species formed (for samples CoCrC and CoCrV) during thermal decomposition taking place prior to the reduction processes.

(d) FT-IR Spectroscopy. The FT-IR spectra of both samples are shown in Figure 5. The broad band at 3355−3395 cm^{-1} is due to the O-H stretching mode of hydroxyl groups, while the medium intensity band at 1618−1634 cm^{-1} is due to the deformation mode of molecular water. The broadness of the first band is in agreement with the existence of hydrogen bonds with different strength (water−carbonate−hydroxyl, water−decavanadate−hydroxyl) in both solids. Lattice modes are responsible for bands below 800 cm^{-1}, and, in addition, other bands are characteristic of the nature of the interlayer anion.

For sample CoCrC, the carbonate bands are shifted and/or split with respect to the spectrum of free carbonate, due to the limited freedom of the anion in the interlayer. Mode ν_3 could be responsible for the sharp band at 1358 cm^{-1}; the splitting giving rise to the shoulder at 1473 cm^{-1} has been previously

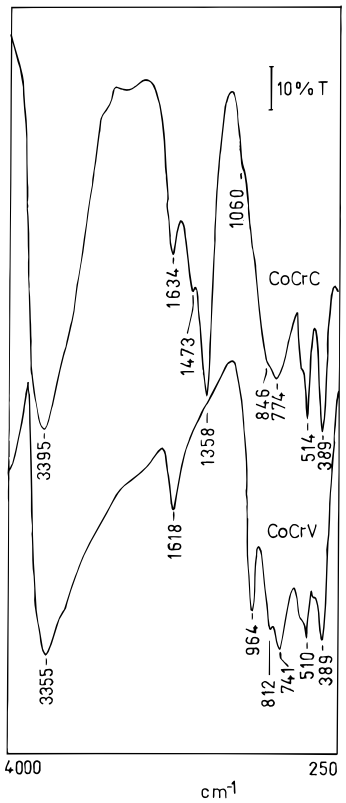

Figure 5. FT-IR spectra of CoCrC and CoCrV hydrotalcites.

reported for other hydrotalcites systems[22,27] and also in aragonite.[28] The very weak shoulder at 1060 cm^{-1} can be ascribed to the totally symmetric stretching mode ν_1; although this mode is IR-forbidden, but Raman-active for free carbonate, the lowered symmetry in the interlayer may activate this mode.[22] The other two bands due to carbonate, out-of-plane (820−900 cm^{-1}) and in-plane (*ca.* 670 cm^{-1}) deformations, are usually overlapped by the lattice bands (mainly involving M−O stretching and M−O−M and O−M−O deformation modes) in the low-wavenumber region of the spectrum. So, ascription of bands to these particular modes is merely tentative and could be done on the shoulder at 846 cm^{-1} (ν_2) and the band at 774 cm^{-1} (ν_4).

The main differences between the spectra of sample CoCrC and sample CoCrV arises from the medium-wavenumber range. The absence of *any* band due to carbonate (1350−1500 cm^{-1}), and even the absence of any shoulder close to 1000−1100 cm^{-1} for sample CoCrV should be stressed. The presence of polyvanadate species accounts for the intense band at 964 cm^{-1}, ascribed to the stretching mode of terminal V═O units.[29] The number and exact position of bands in this region of the spectrum usually gives a clue about the nuclearity of the polyoxometallate.[30] In agreement with V K XANES data reported above for this sample, IR data indicate that vanadium atoms are forming decavanadate anions; bands at 812 and 741 cm^{-1} coincide with other bands reported in the literature for decavanadate.[30] Confirmation of the nuclearity of the polyvanadate[31,32] comes also from the Raman spectrum of this sample; in the 250−400 cm^{-1} range, a single band at 320 cm^{-1} coincides with the position of the band in the Raman spectrum

(26) Rives, V.; Ulibarri, M. A.; Montero, A. *Appl. Clay Sci*. **1995**, *10*, 83.
(27) Bish, D. L. *Abstracts of 6th International Clay Conference*: Pergamon: Oxford, U.K., 1978.
(28) Rives, V.; Munuera, G.; Criado, J. M. *Spectrosc. Lett*. **1979**, *12*, 733.
(29) Frederickson, L. D., Jr.; Hausen, D. M. *Anal. Chem*. **1978**, *23*, 93.
(30) López-Salinas, E.; Ono, Y. *Bull. Chem. Soc. Jpn*. **1992**, *65*, 2465.
(31) Griffith, W. P.; Wickins, T. D. *J. Chem. Soc. A* **1966**, 1087.
(32) Griffith, W. P. *J. Chem. Soc*. *A* **1967**, 905.

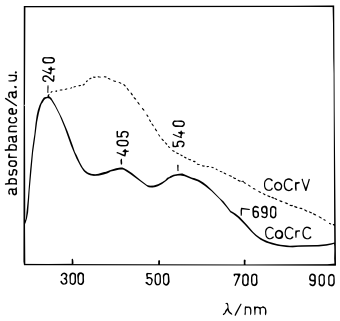

Figure 6. Visible−ultraviolet (diffuse reflectance) spectra of CoCrC and CoCrV hydrotalcites.

of decavanadate in aqueous solution prepared by dissolving $NaVO_3$ at pH 4.5.

(e) Vis−UV Spectroscopy. Although vis−UV spectroscopy is not usually applied to the study of hydrotalcites, we report here some data. The spectra are shown in Figure 6. Since, according to XAS data above, both cations, Co(II) and Cr(III), are located in octahedral sites of the brucite-like layers, the only bands expected in these spectra should correspond to spin-allowed, Laporte-forbidden d−d transitions of the $[CrO_6]$ species (d^3), as the corresponding bands for octahedral $[CoO_6]$ (d^7) are very weak.[33] Two bands at 405 and 540 nm occurring in sample CoCrC, by comparison with the spectrum of $[Cr(H_2O)_6]^{3+}$ (water and oxide are very close in the spectrochemical series), should correspond to transitions $^4A_{2g}(F) \rightarrow {}^4T_{1g}(F)$ and $^4A_{2g}(F) \rightarrow {}^4T_{1g}(F)$, respectively. The weak shoulder at 690 nm can be tentatively ascribed to a spin-forbidden transition, the so-called "ruby line", recorded at 693 nm for ruby.[34] From the equations proposed by Dou,[35] and from the energies of the bands at 405 and 540 nm, the band expected for the third, high-energy, spin-allowed, d−d transition $^4A_{2g}(F) \rightarrow {}^4T_{1g}(P)$ should occur at 252 nm. This should be overlapped by the strong charge transfer band centered at 240 nm. Also the crystal field stabilization energy for $[CrO_6]$ can be calculated as $\Delta_0 = 18\,500\ cm^{-1}$, and the Racah parameter is 591 cm^{-1}.

The spectrum for sample CoCrV is rather different, with a broad, undefined absorption at *ca*. 350 nm and different shoulders, together with the charge transfer band at low wavelengths; as a result, bands due to octahedral units $[CrO_6]$ are not clearly distinguished. However, we conclude that the V^{4+} (d^1) species is absent, as no band is clearly recorded at 600−800 nm.

(f) Texture Properties. The surface texture properties of the samples have been studied by the nitrogen adsorption isotherms at 77 K. The isotherms recorded for both samples correspond to type II of the IUPAC classification,[36] characteristic of nonporous samples. A hysteresis loop, closing at a relative pressure of 0.3, is recorded and can be ascribed to type H2 of the IUPAC classification. The specific surface areas, S_{BET}, calculated following the BET method, are also included in Table 1 and are similar. This result indicates that the nitrogen molecules should not be able to access the interlayer space (probably with a low density of water molecules after the outgassing treatment *in situ* prior to recording the adsorption isotherm), so the specific surface area measured should correspond to external surface. The S_{BET} values also coincide with the values calculated from the *t*-plot.[37] However, it should be mentioned that these plots show a downward deviation for relative pressures above 0.7, indicating the presence of narrow pores that are filled at low relative pressures by multilayer adsorption, thus reducing the surface available for further adsorption at higher pressures.[38] If these narrow pores make up the interlayer volume, it would be expected that the specific surface area would increase on passing from sample CoCrC (with a thickness of the interlayer close to 2.85 Å, taking into account the thickness of the brucite-like layer, 4.8 Å,[6] and the *c/3* parameter for this sample, 7.65 Å) to sample CoCrV (with a thickness of the interlayer space of 6.92 Å, from $c/3 = 11.72$ Å). However, both S_{BET} values are rather close (90 ± 4 $m^2\ g^{-1}$), so the downward deviation of the *t*-plots may be due to adsorption on narrow pores between different stacks of material.

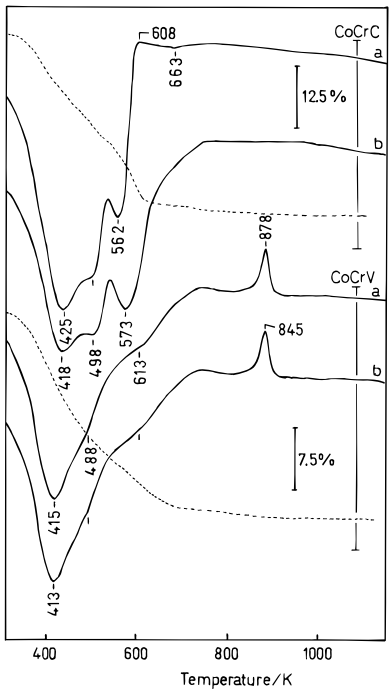

Figure 7. Differential thermal analysis (solid lines) and thermogravimetric analysis (dotted lines) curves for samples CoCrC and CoCrV. Differential thermal analysis curves were recorded in air (a) and in nitrogen (b).

(g) Thermal Analysis. The DTA and TGA curves for samples CoCrC and CoCrV are shown in Figure 7. Two sets of curves are shown for the DTA analysis, one corresponding to the analyses carried out in air (oxidizing conditions) and another recorded in nitrogen (inert atmosphere) in order to detect any changes due to oxidation of the layer cations along the experiments. As expected, the behavior is different in air and in nitrogen. For sample CoCrC, three endothermic peaks are recorded in both cases, positions of which are almost coincident under both experimental conditions: 421 ± 4, 498, and 568 ± 5 K. Despite the intense overlapping of these three peaks (especially between those recorded at lower temperatures), from comparison with the behavior shown by other similar hydrotalcites,[14] the first peak is ascribed to removal of molecular water from the interlayer space, and the two latter peaks are from evolution of CO_2 (from interlayer carbonate) and water vapor, through condensation of hydroxyl groups in the brucite-like layers, as previously shown by mass spectrometry analysis of gases evolved during thermal decomposition of a Mg, Al hydrotalcite.[14]

However, above *ca*. 570 K, the DTA profiles are very different. While in nitrogen, the curve steadily recovers the

(33) Sutton, D. *Espectros electrónicos de los complejos de los metales de Transición*; Reverté: Barcelona, 1975.
(34) Jørgensen, C. K. *Adv. Chem. Phys*. **1963**, *5*, 33.
(35) Dou, Y. *J. Chem. Educ*. **1990**, *67*, 134.
(36) Sing, K. S. W.; Everett, D. H.; Haul, R. A. W.; Moscou, L.; Pierotti, R.; Rouquerol, J.; Sieminiewska, T. *Pure Appl. Chem.* **1985**, *57*, 603.
(37) Lippens B. C.; De Boer J. H. *J. Catal*. **1965**, *4*, 319.
(38) Lowell, S.; Shields, J. E. *Powder Surface Area and Porosity*; Chapman & Hall: London, 1984.

base line, when the analysis is performed in air, the curve shows a sharp increase, yielding an apparent exotherm at 608 K that can be tentatively ascribed to an oxidation process, as this effect is not observed in the nonoxidizing nitrogen atmosphere. A very weak endotherm, absent when the analysis is performed in nitrogen, occurs at 663 K and can be ascribed to a redox process involving Cr(III) ions, as a similar peak has been reported for other hydrotalcite-like systems containing Cr(III) and is absent in specimens without Cr(III).[39−42] This effect has been observed for Ni, Cr[43] and Zn, Cr[44] hydrotalcites and has been ascribed to formation of chromates, Cr(III) → Cr(VI), that at higher temperatures undergo reduction to chromites.

The DTA and TG diagrams for sample CoCrV are shown also in Figure 7. Differences between the profiles recorded in air or in nitrogen are less evident than in the case of sample CoCrC, thus indicating that the nature of the interlayer anion has a marked effect on the evolution of the compounds during calcination. The most intense endotherm, due to removal of water, now occurs at 414 ± 1 K. Two shoulders are seen at *ca.* 488 and 613 K. They cannot correspond to loss of CO_2, as carbonate does not exist in the interlayer, according to the chemical analysis results above mentioned and the FT-IR data. So, these two peaks are due to loss of strongly held water molecules in the interlayer space (probably hydrogen-bonded to the decavanadate units) and to loss of hydroxyl groups from the layers. In both cases, in air and in nitrogen, a sharp exotherm at 862 ± 16 K is observed. The presence of this peak when the experiment is performed under both atmospheres and its position (too high a temperature to be ascribed to a oxidation process similar to that mentioned above for sample CoCrC) and the shape of this peak suggest that it corresponds to a crystallization process.

All TGA diagrams are very similar. Total weight percentage losses from room temperature to 1023 K were 36.7% for sample CoCrC and 31.4% for sample CoCrV. In other hydrotalcite materials[45] the weight loss up to *ca.* 600 K occurs in successive steps that can be ascribed to the progressive loss of water, carbonate, and hydroxyl groups. However, depending on the nature of the layer cations, these steps overlap, as in the present case. In some cases, the weight loss proceeds even above 600−700 K, but the amount of mass lost above this temperature is very low and has been ascribed to removal of residual hydroxyl groups from the layers. The weight loss percentage is larger for sample CoCrC than for sample CoCrV, as expected by taking into account that the interlayer anion of the former is removed as CO_2, but decavanadate persists in the solid even after undergoing some chemical transformation, and the weight loss comes exclusively from interlayer water and layer hydroxyls.

Calcined Materials. Calcination of hydrotalcites at medium temperatures (800 K or above) leads to mixed oxides which are useful catalysts for different processes.[17,46,47] So, in this work we have followed the nature of the products formed upon calcination in air for 2 h at increasing temperatures in 60 K steps. The solids obtained have been characterized using different techniques and have been named as CoCrC-*T* and CoCrV-*T* (for calcined products arising from CoCrC and CoCrV, respectively), where *T* stands for the calcination temperature, in kelvin.

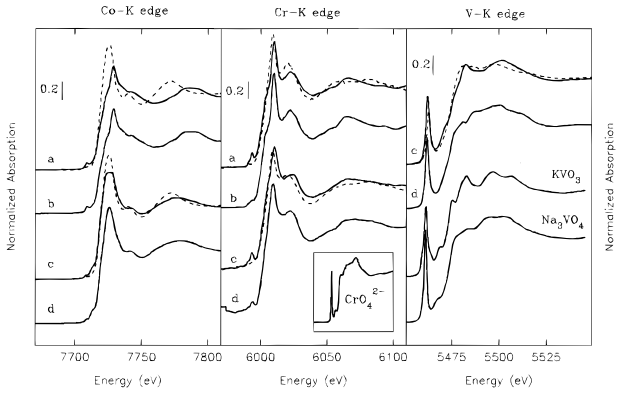

Figure 8. XANES spectra at the Co K, Cr K, and V K edges for samples calcined in air at 673 and 923 K. Data for uncalcined hydrotalcites and reference compounds are also included: (a) CoCrC-673; (b) CoCrC-923; (c) CoCrV-673; (d) CoCrV-923.

Because DTA experiments reported above suggest that redox processes occur after thermal treatments in air, the oxidation state of the cations for selected samples has been studied by XANES spectroscopy. As shown in Figure 8, two inflection points appear at the Co K edge step after calcining CoCrC at 673 K. Also, the most intense maximum in the spectrum is shifted to higher energies when going from the original hydrotalcite to CoCrC-673. These data indicate that a large fraction of Co(II) in the original hydrotalcite is oxidized after calcining at 673 K. Because no further changes are detected after calcination at 923 K, the redox process involving cobalt cations should be complete at 673 K. This oxidation process is not detected for CoCrV, because, as shown in Figure 8, XANES features for calcined CoCrV-673 and CoCrV-923 are similar to those recorded for the uncalcined sample. A small preedge peak appears at the Cr K edge for the calcined samples. This feature, which is absent in the spectrum of the original hydrotalcite, appears at the same energy as that of the characteristic preedge peak of CrO_4^{2-} anions (see inset) and has been assigned to a 1s → 3d electronic transition that is Laporte-forbidden for cations in octahedral coordination, but which becomes partially allowed when the cation is in tetrahedral sites. Data indicate that some Cr(III) cations are oxidized to chromate species after calcining the samples at 673 K, being again partially reduced when the calcination temperature is increased to 923 K. From the intensity of the preedge peak, it is concluded that *ca.* 10% of the original Cr cations is oxidized to chromate in CoCrC-673, while a slightly lower fraction is oxidized in CoCrV-673. The oxidation of Cr(III) to chromates when hydrotalcites that contain this cation are calcined has been previously reported.[39−42] For the Zn(II)−Cr(III) system[44] the oxidation occurs at 473−773 K, and Cr(VI) cations are again reduced when the samples are calcined at higher temperatures.

X-ray diffraction patterns for selected calcined samples are shown in Figure 9. Only the curves for samples where a change in the nature of the crystalline phases is observed have been included. For sample CoCrC-433, the layered structure is partially preserved, although basal spacing slightly decreases, probably due to partial removal of interlayer water molecules, and diffraction peaks broaden, indicating a lower crystallinity of the material. However, the layered structure is completely destroyed when the sample is calcined at 493 K, leading to a sample in which weak diffraction peaks due to Co_2CrO_4 are

(39) Gusi, S.; Pizzoli, F.; Trifiro, F.; Vaccari, A.; Del Piero, G. *Stud. Surf. Sci. Catal.* **1987**, *31*, 753.
(40) Del Piero, G.; Di Conca, M.; Trifiro, F.; Vaccari, A. In *Reactivity of solids*; Barret, P., Dufour, L. C., Eds.; Elsevier: Amsterdam, 1985; p 1029.
(41) Yamaguchi, O.; Taguchi, H.; Miyata, Y.; Yoshinaka, M.; Shimizu, K. *Polyhedron* **1987**, *6*, 1587.
(42) Sato, T.; Fujita, H.; Endo, T.; Shimada, M. *React. Solids* **1988**, *5*, 219.
(43) Clause, O.; Gazzano, M.; Trifiro, F.; Vaccari, A.; Zatorski, L. *Appl. Catal.* **1991**, *73*, 217.
(44) Fuda, K.; Suda, K.; Matsunaga, T. *Chem. Lett.* **1993**, 1479.
(45) Chisen, I. C.; Jones, W. *J. Mater. Chem.* **1994**, *4*, 1737.
(46) Uzunova, E.; Klissurski, D.; Kassabov, S. *J. Mater. Chem.* **1994**, *4*, 153.
(47) Climent, M. J.; Corma, A.; Iborra, S.; Primo, J. *J. Catal.* **1995**, *151*, 60.

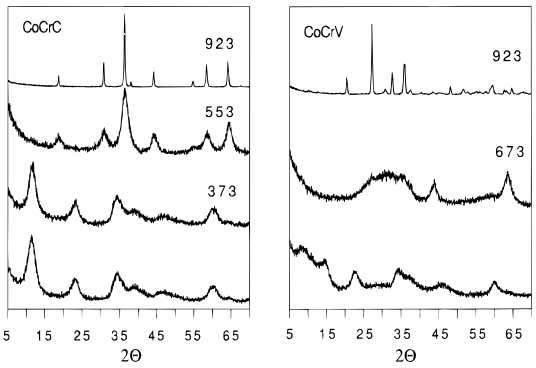

Figure 9. X-ray diffraction patterns of CoCrC and CoCrV and calcined in air at the temperatures given (K).

identified, these peaks being better resolved (*i.e*, this phase being better crystallized) after calcination at 553 K. When the calcination is performed at higher temperatures, a mere improvement in the crystallinity of the samples (denoted by sharper and more intense diffraction peaks) is observed.

Calcination of sample CoCrV at 433 K has no effect on the general features of the diffraction pattern, peaks being in the same positions but slightly less intense. After calcination at 493 K, peaks due to the layered material are almost completely removed, and a very broad feature, extending from 3.3 to 2.44 Å, is seen, along with ill-definded maxima at 3.04 and 2.57 Å. A similar behavior upon thermal decomposition of polyoxovanadate-containing Mg, Al hydrotalcite has been described by Twu and Dutta.[48] These authors suggest that decomposition of decavanadate starts above 373 K, leading to smaller, cyclic $V_3O_9^{3-}$ species, thus accounting for the decrease in the interlayer spacing. From Raman spectroscopy results, these authors conclude that calcination between 433 and 553 K leads to depolymerization of decavanadate according to reaction:

$$V_{10}O_{28}^{6-} + 3H_2O \rightarrow 3V_3O_9^{3-} + HVO_4^{2-} + 5H^+$$

When our sample is calcined at 553 and 613 K, the layered structure collapses and no defined peak is recorded in the XRD diagram; i.e., it corresponds to mostly amorphous solids. Weak peaks are, however, seen at 1.47 and 2.06 Å, together with a broad feature between 3.4 and 2.6 Å, whose intensities increase with the calcination temperature. The first two peaks become stronger after calcination at 673 K and can be ascribed to ill-crystallized $CoCr_2O_4$. No peak due to diffraction by vanadate-containing species is recorded. When the sample is calcined at 733 K or above, the diffraction diagrams are absolutely different, with sharp, intense diffraction peaks due to $CoCr_2O_4$ and $Co_2V_2O_7$.

The V K XANES obtained for sample CoCrV-673, Figure 8, is similar to that recorded for a crystalline metavanadate (KVO_3) where [VO_4] tetrahedra form a chain anion (α-VO_3^-) by sharing vertices.[49] These data indicate that similar chains are also formed in CoCrV-673 through the polymerization reaction:

$$nV_3O_9^{3-} \rightarrow 3[-(VO_3^-)-]$$

After calcining at 923 K, the V K XANES is closer to that obtained for a crystalline orthovanadate (Na_3VO_4), where V^{5+} cations form monomeric tetrahedral units, VO_4^{3-}. This result indicates that the α-VO_3^- chains detected in CoCrV-673 have depolymerized after calcining at 923 K and agrees with the detection of $Co_2V_2O_7$ by XRD, since in this compound only two [VO_4] units share a vertex to form the dimer $V_2O_7^{4-}$.[50]

Table 3. Structural Parameters from EXAFS for Selected Calcined Samples[a]

bond	N	$\Delta\sigma^2 \times 10^3$	R (Å)	$\Delta E°$ (eV)
		CoCrC-673		
Co−O	4.3	3.7	1.93	−0.5
Co−M	4.7	7.3	2.88	0.1
Co−M	4.4	2.0	3.38	5.9
Cr−O	6.0	5.0	1.98	9.9
Cr−M	5.8	6.2	2.94	11.0
Cr−M	1.5	2.9	3.41	10.6
		CoCrC-923		
Co−O	4.3	3.7	1.93	−0.5
Co−M	4.7	7.3	2.88	0.1
Co−M	5.5	2.0	3.38	5.9
Cr−O	6.0	3.6	1.97	9.8
Cr−M	5.1	2.6	2.94	11.0
Cr−O	2.1	2.2	3.43	10.6
		CoCrV-673		
Co−O	4.9	8.4	2.01	4.6
Co−M	2.2	8.0	3.00	−0.3
Co−M	0.9	1.8	3.38	7.7
		CoCrV-923		
Co−O	5.6	7.4	2.04	2.6
Co−M	1.5	8.0	3.07	−7.3
Co−M	1.2	1.8	3.38	7.7

[a] Estimated error for coordination numbers (N) and bond lengths (R) are ±10% and ±0.02 Å, respectively. Unfiltered experimental data were fitted (fit range 3−12 $Å^{-1}$ at the Co K edge and 3.4−11.9 $Å^{-1}$ at the Cr K edge).

From this study it can be concluded that changes in both samples under calcination in air are rather similar, leading to formation of low-crystallinity solids at intermediate temperatures. When the calcination temperature is raised, crystalline compounds are formed, whose nature (even regarding phases containing the cations originally existing in the layers) depends on the parent hydrotalcite-like solid. So, samples CoCrC-*T* undergo partial oxidation Co(II) → Co(III) and crystallization of Co_2CrO_4 (this compound can be formulated as $Co^{II}Co^{III}Cr^{III}O_4$). However, calcination of sample CoCrV takes place without this oxidation process and leads to formation of spinel $CoCr_2O_4$ (*i.e*., $Co^{II}Cr^{III}_2O_4$), together with $Co^{II}_2V^{V}_2O_7$.

The local order around Co and Cr cations was studied by EXAFS spectroscopy in samples calcined at 673 and 923 K. XRD data indicated that in both samples, CoCrC-923 and CoCrV-923, the phases formed are well-crystallized. Parameters obtained by best-fit procedures are collected in Table 3, while representative examples of experimental data and fit functions are shown in Figure 10. From comparison of shell radii included in Table 3, which only depend on the precursor sample and which are independent of the calcination temperature, it is concluded that amorphous phases present in the samples calcined at 673 K have a local structure around Co and Cr cations similar to that found in the crystalline phases formed after calcination at 973 K.

Coordination parameters for Cr(III) cations in CoCrC calcined at 673 or 923 K show that all the metal ions are located in octahedral holes in agreement with the parameters expected for the spinel Co_2CrO_4 (see Table 4). Although XRD data cannot distinguish the distribution of Co(II), Co(III), and Cr(III) cations between tetrahedral and octahedral lattice sites, Hank and Laitinen[51] proposed a lattice structure similar to that reported

(48) Twu, J.; Dutta, P. K. *J. Catal*. **1990**, *124*, 503.
(49) Wells, A. F. *Structural Inorganic Chemistry*, 4th ed.; Clarendon Press: Oxford, U.K., 1975.
(50) Sallerbrei, E. E.; Faggiani, R.; Calvo, C. *Acta Crystalllogr. B* **1974**, *30*, 2907.
(51) Hank, K. W.; Laitinen, H. A. *J. Inorg. Nucl. Chem.* **1971**, *33*, 63.
(52) Garcia Casado, P.; Rasines I. *Poyhedron* **1986**, *5*, 787.

Table 4. Coordination Parameters for Crystalline Compounds[50−52]

Co_2CrO_4				$CoCr_2O_4$				$Co_2V_2O_7$	
Co(II)		Cr(III)/Co(III)		Co(II)		Cr(III)		Co(II)	
4 *O*	1.942 Å	6 *O*	1.917 Å	4 *O*	1.963 Å	6 *O*	1.996 Å	6 *O*	2.08 Å
12 *Co/Cr*	3.351 Å	6 *Co/Cr*	2.858 Å	12 *Cr*	3.455 Å	6 *Cr*	2.947 Å	2.5 *Co*	3.03 Å
4 *Co*	3.500 Å	6 *Co*	3.351 Å	4 *Co*	3.609 Å	6 *Co*	3.455 Å	6.5 *V*	3.33−3.53 Å

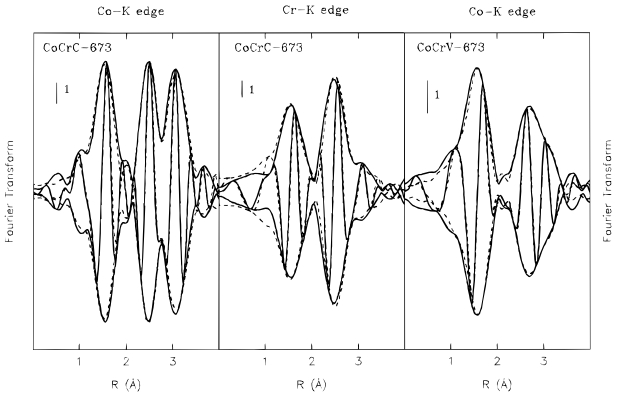

Figure 10. EXAFS data for samples CoCrC-673 and CoCrV-673. Modulus and imaginary part of the k^3-weighted Fourier transforms. Solid lines: unfiltered experimental data. Dashed lines: best-fit functions. $\Delta k = 3-12$ Å^{-1} at Co K edge. $\Delta k = 3.4-11.9$ Å^{-1} at Cr K edge.

for Co_3O_4,[53] where half of the Co(III) cations have been exchanged by Cr(III). Thus, tetrahedral positions are occupied by Co(II) and the octahedral positions shared by Co(III) and Cr (III) cations. Also, the lattice parameter of Co_2CrO_4 (a = 8.11 Å) is close to that for Co_3O_4 (a = 8.17 Å), and therefore coordination numbers and bond lengths given in Table 4 for Co_2CrO_4 were calculated from structural parameters reported for Co_3O_4.

Experimental bond lengths for coordination shells around Co cations (Table 3) also agree with the average values deduced for Co_2CrO_4 from crystallographic data. However, the value obtained for the number of oxygen atoms (4.3) in the first coordination shell is lower than that expected (5.0) for the normal spinel structure, where Co(II) and Co(III) cations occupy the tetrahedral and octahedral lattice sites, respectively, while the experimental coordination number at 2.88 Å (4.7 cobalt cations) is higher than the average value at this distance for cobalt cations in crystalline Co_2CrO_4 (three Co−M interactions at 2.858 Å).

Regarding samples obtained by calcination of the parent CoCrV, XRD detected formation of two crystalline compounds, $CoCr_2O_4$ and $Co_2V_2O_7$. Shell radii determined from EXAFS data for the coordination spheres of cobalt (Table 3) are those expected for a mixture of both compounds (see Table 4 for parameters calculated from crystallographic data). The stoichiometry of the starting precursor, $[Co_{0.61}Cr_{0.39}(OH)_2](V_{10}O_{28})_{0.065}$, establishes that if all chromium atoms were forming crystalline $CoCr_2O_4$, 31% of Co atoms could be in this phase. On the other hand, enough vanadium is present to react stoichiometrically with Co to produce $Co_2V_2O_7$. Because Co cations are in octahedral holes in the latter compound (see Table 4), while they are located in tetrahedral sites in the $CoCr_2O_4$ normal spinel lattice, the average oxygen coordination number in the first shell should be ≥5.4, in agreement with the experimental value in Table 3 for CoCrV-923. However, this coordination number decreases to 4.9 for sample CoCrV-673, indicating that, in this sample, there are more cobalt cations than expected in tetrahedral coordination. It is worth noting that for CoCrV-673 a coordination number of 2.2 is obtained from EXAFS data for Co−M bonds at 3 Å, a Co−M shell radii characteristic of crystalline $Co_2V_2O_7$ with an average coordination number of 2.5 for the crystalline material. This result is surprising because XRD, XANES, and FT-IR data above showed that crystalline $Co_2V_2O_7$ was not formed in CoCrV-673 and that most of the vanadium cations occurred as amorphous metavanadate chains in this sample. Moreover, the Co−M coordination number at 3 Å (determined from EXAFS data) decreased to 1.5 in CoCrV-923, where XRD showed that crystalline $Co_2V_2O_7$ was undoubtedly formed.

Therefore, structural data obtained from EXAFS data indicate that in CoCrC-673, CoCrC-923, and CoCrV-923 there are more cobalt cations in tetrahedral sites and more Co−M bonds at 2.9−3.0 Å than the values expected on the basis of the exclusive formation of stoichiometric compounds. Results reported in the literature[40,54−58] on the thermal decomposition of NiAl, ZnCr, and ZnAlCuCo hydrotalcites were explained by assuming the presence of an excess of divalent cations dissolved in the spinel phase. Our structural data suggest that a similar phenomenon occurs during calcination at 673 K of CoCrC and CoCrV hydrotalcites and that the spinel phases formed are nonstoichiometric, having an excess of Co(II) cations in tetrahedral holes. This phase is stable in CoCrC-973, while for CoCrV-973 it decomposes, probably due to the reaction of the excess cobalt to yield vanadates.

The FT-IR spectra of representative samples CoCrC-*T* are shown in Figure 11. Only the wavenumber range where changes are expected are shown. Calcination below 433 K does not give rise to important changes in the spectrum, only a decrease in the intensities of the stretching and deformation bands of water molecules. The peak at 1355 cm^{-1} with a shoulder at 1470 cm^{-1}, due to mode ν_3 of interlayer carbonate species in the original, uncalcined sample, however, undergoes important changes. The shoulder shifts above 1500 cm^{-1}, and its intensity increases for samples calcined at 433 and 493 K; above this temperature these peaks vanish, due, in agreement with the TGA data, to complete removal of carbonate species. This behavior is similar to that previously observed during calcination of hydrotalcite materials containing Mg^{2+} and Cr^{3+}, or Mg^{2+} and V^{3+} in the layers,[59] and the peaks still recorded have been ascribed to surface-adsorbed carbonate.[60] Changes also occur in the 250−1000 cm^{-1} range, where absorptions due to modes ν_2 and ν_4 of carbonate and to lattice vibrations occur. Bands become broader and less intense as the calcination temperature increases, but at higher calcination temperatures

(53) Knop, O.; Erid, K.; Nagakawa, Y. *Can. J. Chem.* **1968**, *46*, 3463.
(54) Puxley, D. C.; Kitchener, I. J.; Komodromos, C.; Parkyns, N. D. *Stud. Surf. Sci. Catal.* **1983**, *16*, 237.
(55) Del Piero, G.; Trifiro, F.; Vaccari, A. *J. Chem. Soc., Chem. Commun.* **1984**, 656.
(56) Bertoldi, M.; Fubini, B.; Giamello, E.; Busca, G.; Trifiro, F.; Vaccari, A. *J. Chem. Soc., Faraday Trans. 1*, **1988**, *84*, 1405.
(57) Di Conca, M.; Riba, A.; Trifiro, F.; Vaccari, A.; Del Piero, G.; Fattore, V.; Pincilini, F. *Proceedings of the 8th International Congress on Catalysis*; Dechema: Frankfurt, Germany, 1984; Vol. II, p 173.
(58) Marchi, A. J.; Di Cosimo, J. I.; Apesteguia, C. R. In *Proceedings of the 9th International Congress on Catalysis;* Phillips, M. J., Ternan, M., Eds.; The Chemical Institute of Canada: Ottawa, 1988, Vol. 3, p 529.
(59) Martín Labajos, F. M. Ph.D. Thesis, University of Salamanca, 1993.
(60) Serna, C. J.; White, J. L.; Hem, S. L. *Soil Sci. Soc. Am. J.* **1977**, *41*, 1009.

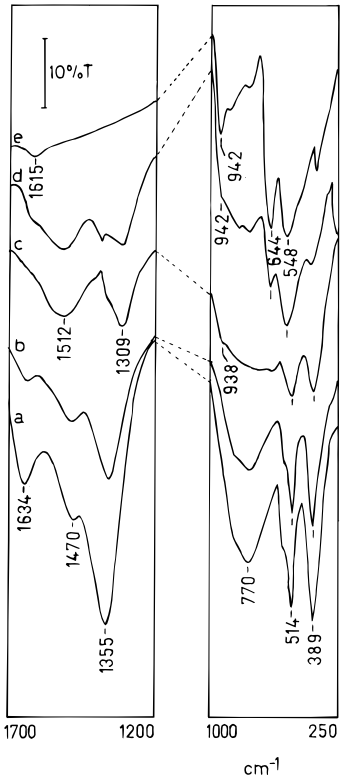

Figure 11. FT-IR spectra of (a) CoCrC and that calcined in air at (b) 373, (c) 433, (d) 493, and (e) 533 K.

(where XRD indicates crystallization of new phases) sharp bands again develop. Although the infrared spectrum of spinel Co_2CrO_4 has not been reported in the literature, data for similar compounds[61,62] suggest that the three bands at 644, 548, and 370 cm^{-1} can be ascribed to modes ν_1, ν_2, and ν_3 of this structure; mode ν_4 is below the wavenumber range covered by our instrument.

Spectra for samples obtained after calcination of parent sample CoCrV, Figure 12, are shown only in the 250−1000 cm^{-1} range, as bands due to polyvanadate are expected in this range. In addition, other changes in the spectra (removal of water and hydroxyl groups) follow the expected pattern, also found for sample CoCrC. Band broadening is observed after calcination at 373 K, although two peaks, characteristic of polyvanadate species, are still seen at 965 and 747 cm^{-1}; the shoulder at 665 cm^{-1}, which intensity increases with the calcination temperature, has been previously ascribed[30] to $H_xV_{10}O_{28}^{x-6}$ ($x = 1, 2, 3$). Decavanadate-derived bands disappear after calcination at 433 K, and the spectrum is then dominated by a broad band between 950 and 650 cm^{-1} for all samples calcined below 673 K. From this temperature upward, peaks at 530, 675, and 920 cm^{-1} are ascribed to chain-polymers $(-VO_3-)_n$.[30] When the sample is calcined above 673 K, the peaks due to $Co_2V_2O_7$, the presence of which has been identified by X-ray diffraction, occur at 893 and 670 cm^{-1}.

The UV−vis spectra confirm the partial oxidation Co(II) → Co(III). For samples CoCrC-*T* ($T \geq 433$ K), an almost constant absorption is observed in the visible range, with weak maxima at 670 and 380 nm coincident with those of Co_3O_4 (the solid is completely black), although this species has not been detected by XRD.

The TPR profiles of the calcined samples are shown in Figure 13 and Figure 14. For comparison, the profiles for the uncalcined samples have been also included.

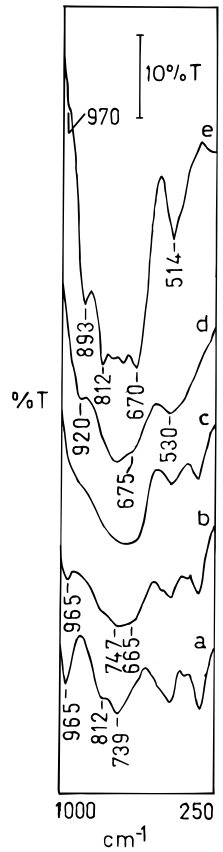

Figure 12. FT-IR spectra of (a) CoCrV and that calcined in air at (b) 373, (c) 433, (d) 673, and (e) 823 K.

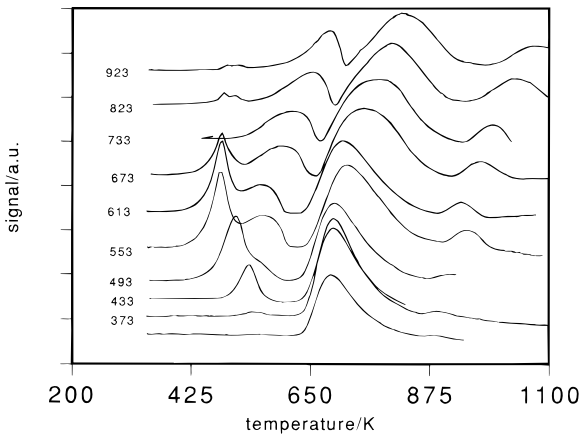

Figure 13. Temperature-programmed reduction profiles of CoCrC and calcined in air at the temperatures given (K).

Reduction profiles for samples CoCrC-*T* show a main reduction peak close to 673 K, and it steadily shifts toward higher temperatures as the calcination temperature is increased. Such an effect is usually ascribed to formation of crystalline species, whose reduction takes place at higher temperatures than for amorphous phases. In addition, some features appear at lower temperatures. The intensity of the sharp peak centered around 470 K increases with the calcination temperature and then decreases. In addition, the broad peak at 543 K for sample CoCrC-553 (although a shoulder in this position is already recorded for sample CoCrC-493) shifts up to 679 K for sample CoCrC-923 K. Unfortunately, we did not record the XAS of all these samples in order to ascertain the nature of the species responsible for these reduction peaks. However, XAS data indicate formation of Co^{3+} in sample CoCrC-673 (the Co^{3+} concentration seems to be unaltered in samples calcined at higher temperatures, CoCrC-923). In addition, oxidized Cr^{n+} species

(61) Preudhomme, J.; Tarte, P. *Spectrochim. Acta* **1971**, *27A*, 1817.
(62) Preudhomme, J.; Tarte, P. *Spectrochim. Acta* **1972**, *28A*, 69.

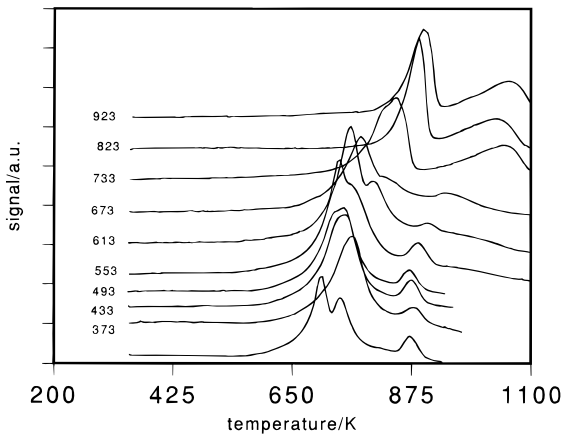

Figure 14. Temperature-programmed reduction profiles of CoCrV and calcined in air at the temperatures given (K).

($n > 3$) are also formed at intermediate calcination temperatures, decomposing when the samples are heated to higher temperatures. So, as the broad peak at 543−679 K is recorded even for sample CoCrC-923, but the sharp peak at *ca.* 470 K is absent for this sample, we tentatively ascribe these two peaks to reduction of chromate-like species (sharp peak) and of Co^{3+} species (to Co^{2+} species) the broad peak. It should be noted that TPR analysis of hydrotalcite-like materials containing Ni and Cr, precalcined at increasing temperatures, also showed development (and disappearance) of similar sharp peaks in this same temperature range.[26]

Reduction profiles for samples CoCrV-*T* are shown in Figure 14. In all cases, a main reduction peak at 725 K (that shifts toward high temperatures as the precalcination temperature increases) and a small one at *ca*. 870 K are recorded. Data for Mg, Al hydrotalcite containing decavanadate (*i.e.*, a sample where the only reducible cation is V^{5+} in decavanadate) indicate that this reduces at 897 K,[26] so the small peak should be due to reduction of the decavanadate species originally existing in the interlayer space. It should be noted that a peak with a similar intensity was also observed during TPR analysis of samples CoCrC-*T* precalcined at or above 553 K (see Figure 13); however, in this case the peak cannot be ascribed to reduction of vanadate, as this anion does not exist in samples CoCrC. In this series of samples the peak is only recorded in precalcined samples (while for series CoCrV-*T* it appears even for the uncalcined sample), we conclude that this peak, for samples CoCrC-*T* ($T \geq 553$), should originate from hardly reducible Co^{n+} species. So, the main reduction peak around 725 K is due to reduction of Co^{2+} species.

Quite interestingly, no reduction peak is recorded in any case below the reduction peak close to 725 K, in agreement with previous XAS experiments, Co^{3+} species are not formed in this series of samples. The absence of detectable Cr^{n+} species ($n > 3$) in our TPR experiments, a small fraction of which has been detected by XAS for samples CoCrV-*T* calcined at intermediate samples, could be due to a lower sensitivity of TPR if compared to that of XAS.

The nitrogen adsorption isotherms for samples CoCrC-*T* and CoCrV-*T* correspond to type II in the IUPAC classification,[36] with hysteresis loops closing at $P/P_0 = 0.3$, except for samples CoCrC-533 and CoCrC-933 and samples CoCrV-*T* ($T \geq 673$ K), which are almost reversible. Hysteresis corresponds to type H2 for samples calcined below 673 K but changes to type H3 for samples calcined at higher temperatures. Most probably, this change corresponds to crystallization of Co_2CrO_4 and $CoCr_2O_4$ which was detected by X-ray diffraction. The change in the specific surface areas of the samples with the calcination temperature has been plotted in Figure 15. Uncalcined samples present similar values, as above discussed. When the samples are calcined at *ca.* 500 K, they exhibit the largest specific surface areas and then decrease steadily as the calcination temperature is further increased. Maximum specific surface areas correspond to formation of amorphous materials, as concluded from X-ray dffraction studies. However, it should be stressed that although both samples exhibit their highest specific surface area values when calcined at 493 K, the specific surface area of sample CoCrC-493 is more than twice the value measured for sample CoCrV-493. Surface area development for calcined carbonate-containing LDH has been explained[63] on the basis of formation of small craters through the brucite-like layers, formed by CO_2 escaping from the interlayers. Such a mechanism would also be possible in our calcined CoCrC samples, but not in CoCrV samples.

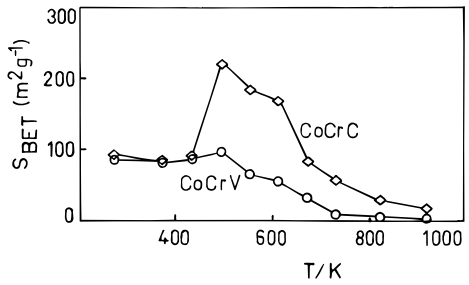

Figure 15. Change in the specific surface area of CoCrC and CoCrV with calcination temperature.

Conclusions

Hydrotalcites containing Co(II) and Cr(III) in the brucite-like layers have been prepared, with carbonate or decavanadate in the interlayers. In both cases, cobalt remains as Co(II), without any oxidation to Co(III).

According to results, mainly by XAS and FT-IR spectroscopies, vanadium exists as decavanadate, both in the interlayer and as a salt phase.

When the samples are calcined at increasing temperature in air, Co(II) becomes oxidized to Co(III) in sample CoCrC, but such an oxidation does not take place in sample CoCrV. Chromium undergoes an oxidation/reduction process in both samples but more intense in sample CoCrC.

Calcination leads to formation of amorphous materials at intermediate temperatures, and at high temperatures crystallization leads to formation of spinel Co_2CrO_4 (when starting from hydrotalcite CoCrC), but $CoCr_2O_4$ when starting from hydrotalcite CoCrV; in this case, formation of $Co_2V_2O_7$ is also observed.

Acknowledgment. Financial support from CICYT (Grant MAT93-0787) and Consejeria de Cultura y Turismo de la Junta de Castilla y León (Spain) are greatly acknowledged. Authors also thanks Mr. A. Montero for measurement of the specific surface areas of the samples. Authors thank Prof. P. Román (UPV-EHU) the gift of of *n*-hexylammonium hexavanadate.

IC9601551

(63) Reichle, W. R.; Kang, S. Y.; Everhardt, D. S. *J. Catal.* **1986**, *101*, 352.